Abdominal Radiology

Published online: 28 June 2018

Abdom Radiol (2019) 44:131–139
https://doi.org/10.1007/s00261-018-1684-z

Intravoxel incoherent motion diffusion-weighted MR imaging of solid pancreatic masses: reliability and usefulness for characterization

Riccardo De Robertis,[1] Nicolò Cardobi,[1] Silvia Ortolani,[2] Paolo Tinazzi Martini,[1] Alto Stemmer,[3] Robert Grimm,[3] Stefano Gobbo,[4] Giovanni Butturini,[5] and Mirko D'Onofrio[1]

[1]Department of Radiology, Ospedale P. Pederzoli, Via Monte Baldo, 24, 37019 Peschiera del Garda, Italy
[2]Department of Oncology, Ospedale P. Pederzoli, Via Monte Baldo, 24, 37019 Peschiera del Garda, Italy
[3]Siemens Healthcare, Allee am Roethelheimpark, 2, 91052 Erlangen, Germany
[4]Department of Pathology, Ospedale P. Pederzoli, Via Monte Baldo, 24, 37019 Peschiera del Garda, Italy
[5]Department of Pancreatic Surgery, Ospedale P. Pederzoli, Via Monte Baldo, 24, 37019 Peschiera del Garda, Italy

Abstract

Purpose: IVIM-DW imaging has shown potential usefulness in the study of pancreatic lesions. Controversial results are available regarding the reliability of the measurements of IVIM-derived parameters. The aim of this study was to evaluate the reliability and the diagnostic potential of IVIM-derived parameters in differentiation among focal solid pancreatic lesions and normal pancreas (NP).
Methods: Fifty-seven patients (34 carcinomas—PDACs, 18 neuroendocrine neoplasms—panNENs, and 5 autoimmune pancreatitis—AIP) and 50 subjects with NP underwent 1.5-T MR imaging including IVIM-DWI. Images were analyzed by two independent readers. Apparent diffusion coefficient (ADC), slow component of diffusion (*D*), incoherent microcirculation (Dp), and perfusion fraction (*f*) were calculated. Interobserver reliability was assessed with intraclass correlation coefficient (ICC). A Kruskal–Wallis *H* test with Steel–Dwass post hoc test was used for comparison. The diagnostic performance of each parameter was evaluated through receiver operating characteristic (ROC) curve analysis.
Results: Overall interobserver agreement was excellent (ICC = 0.860, 0.937, 0.968, and 0.983 for ADC, *D*, Dp, and *f*). *D*, Dp, and *f* significantly differed among PDACs and panNENs ($p = 0.002$, < 0.001, and < 0.001), albeit without significant difference at the pairwise comparison of ROC curves ($p = 0.08$-0.74). Perfusion fraction was higher in AIP compared with PDACs ($p = 0.024$; AUC = 0.735). Dp and *f* were higher in panNENs compared with AIP ($p = 0.029$ and 0.023), without differences at ROC analysis ($p = 0.07$).
Conclusions: IVIM-derived parameters have excellent reliability and could help in differentiation among solid pancreatic lesions and NP.

Key words: Pancreas—Intravoxel incoherent motion—Diffusion-weighted imaging—Pancreatic carcinoma—Magnetic resonance imaging

Diffusion-weighted (DW) imaging has been increasingly used over the last few years for the evaluation of the pancreas during magnetic resonance (MR) examinations [1–6]. DW imaging improves identification of pancreatic lesions [2, 4, 5]; moreover, quantitative analysis of DW images with the determination of the apparent diffusion coefficient (ADC) value may provide ancillary findings that could predict the clinical behavior of pancreatic tumors [7–9]. However, since ADC is affected by both molecular diffusion and blood flow, it may not be reliable for tissue characterization; as several previous studies have reported a wide overlap between the ADC values of different pancreatic lesions, the usefulness of DW imaging for differentiation of solid lesions of the

Correspondence to: Riccardo De Robertis; *email:* riccardo.derobertis@hotmail.it

pancreas is still debated [1, 3, 10]. Intravoxel incoherent motion (IVIM) imaging relies on the use of multiple *b*-values and models DW signal as the sum of two exponential curves, thereby enabling the quantification of the relative contribution of perfusion and true molecular diffusion to the random motion of water molecules within biological tissues and thus improving tissue characterization [11, 12]. Previous studies have shown potential of IVIM-DW imaging in the study of pancreatic lesions [13–20]. For instance, it has been reported that pancreatic ductal adenocarcinoma (PDAC) and pancreatic neuroendocrine neoplasms (panNENs) can be differentiated using perfusion-related IVIM-derived parameters [15, 16, 20] and that the perfusion fraction (*f*) is more reliable than ADC for differentiating mass-forming pancreatitis (MFP) and PDACs [14]. However, these results are mainly derived from experimental studies and are based on relatively small populations; therefore, they should be considered preliminary. For instance, little is still known about the real capability of IVIM-DW imaging in differentiating inflammatory mass-forming masses from pancreatic tumors. The aim of this study was to evaluate the reliability and the diagnostic potential of IVIM-derived parameters in the differentiation of focal solid pancreatic lesions including PDAC, panNENs, autoimmune pancreatitis (AIP), and normal pancreas (NP).

Materials and methods

Subjects

This study was approved by our Institutional Review Board. Signed informed consent was obtained before MR examinations. Four hundred consecutive patients with a known pancreatic mass previously seen in US or CT underwent MR imaging including IVIM-DW between July 2016 and July 2017. Inclusion criteria were: (a) focal solid pancreatic lesion; (b) pathological confirmation of pancreatic neoplasm after surgical resection or fine-needle aspiration or diagnosis of autoimmune pancreatitis as defined by international consensus guidelines [21]; (c) good-quality MR examination (i.e., absence of major motion artifacts or misregistration artifacts on IVIM-derived maps). Patients with the following criteria were excluded: (a) cystic pancreatic lesion; (b) lack of pathologic data; (c) MR images of poor quality owing to the presence of motion artifacts or misregistration artifacts. A control group of subjects with normal pancreas, who underwent MR for abdominal—other than pancreatic—diseases, were also included; the diagnosis of normal pancreas in this group was assigned on the basis of a combination of (a) no documented history of pancreatic disease; (b) no abnormal radiologic signs in the pancreas at MR imaging; (c) no clinical and biochemical features of pancreatic disease.

Image acquisition

All examinations were performed on a 1.5 Tesla MR unit (MAGNETOM Aera, Siemens Healthcare, Erlangen, Germany) by using a multichannel phased-array coil. MR parameters are presented in Table 1.

T2- and unenhanced T1-weighted images were obtained by using the half-Fourier acquisition single-shot turbo spin echo (HASTE) sequence and the Dixon sequence, respectively. MR cholangiopancreatography images were obtained by using breath-hold single-section rapid acquisition with turbo spin echo (TSE). IVIM-DW images were obtained before contrast medium administration. Spectral presaturation attenuated by inversion recovery (SPAIR) was used for fat suppression. DW images were acquired by using a prototype single-shot echo-planar imaging (SS-EPI) pulse sequence during free breathing with parallel imaging and *b*-values of 0, 10, 20, 30, 50, 70, 100, 150, 200, 400, and 800 s/mm^2. Dynamic images were obtained by using a fat-suppressed three-dimensional volume interpolation with breath-hold examination (VIBE) sequence; dynamic study was performed before and after administration of gadopentate dimeglumine (Multihance; Bracco; Milan, Italy) at a dose of 0.1 mmol/mL with an injection rate of 2 mL/s. Arterial, portal venous, and delayed phase images were obtained at 30–40 s, 60–65 s, and 180 s, respectively, after contrast medium injection.

Image analysis

The analysis of IVIM-DW images was performed independently by two radiologists (R.D.R. and N.C., with 8 and 7 years of experience in abdominal MR imaging interpretation, respectively) blinded to the final diagnosis and to each other's measurements. DW data were post-processed using a dedicated prototype software (MR Body Diffusion Toolbox, version 1.3.0; Siemens Healthcare, Erlangen, Germany), which automatically computed ADC maps through a mono-exponential model and IVIM parametric maps using a bi-exponential modeling with full non-linear fitting of IVIM-derived parameters. Multiple freehand regions of interest (ROIs) were drawn on all contiguous axial slices containing the lesion on DW images, using T2-weighted and contrast-enhanced MR images as the anatomic reference to identify the extent of each lesion. ROIs were then directly co-localized on IVIM-derived parameter maps. For quantitative analysis in the control group, three circular ROIs were drawn in the pancreatic parenchyma at the head, the body, and the tail. The median value of the measurements defined each measured parameter.

Table 1. MR imaging acquisition protocol

Sequence and imaging plane	TR/TE (ms)	Field of view (mm)	Matrix	Flip angle (degrees)	Section thickness (mm)	Voxel size (mm)
T2w HASTE						
Axial	∞/90	400–450	512 × 384	180	6	1 × 1 × 6
Coronal	∞/90	400–450	364 × 384	180	6	1 × 1 × 6
Sagittal	∞/90	390–400	253 × 512	180	4	1 × 1 × 4
IVIM-DW EPI axial[a]	6000/59	400–440	192 × 144	90	6	2.3 × 2.3 × 6–6.5
T2w TSE FS axial	2900/82	400–460	384 × 174	160	6	1.1 × 1.1 × 6–6.5
T1w Dixon axial	6.69/2.39–4.77	400–430	320 × 173	10	3–3.5	1.2 × 1.2 × 3–3.5
T1w FS VIBE						
Axial	6.1/2.4	400–480	320 × 256	10	3–3.5	1.2 × 1.2 × 3–3.5
Coronal	6.1/2.4	400–450	187 × 256	10	3	1.2 × 1.2 × 3
2D MRCP	∞/746	300	384 × 384	180	70	0.8 × 0.8 × 70

[a]Acquired during free breathing; 11 *b*-values were used (0, 10, 20, 30, 50, 70, 100, 150, 200, 400, and 800 s/mm^2)
TR, repetition time; TE, time of echo; T2w, T2-weighted; HASTE, half-Fourier acquisition single-shot turbo spin echo; IVIM, intravoxel incoherent motion; DW, diffusion-weighted; EPI, echo-planar imaging; TSE, turbo spin echo; FS, fat suppressed; T1w, T1-weighted; VIBE, volume-interpolated breath-hold examination; MRCP, magnetic resonance cholangiopancreatography

Statistical analysis

Interobserver reliability of the measurements was assessed by using the intraclass correlation coefficient (ICC): ICC values lower than 0.40 indicated poor reliability; ICC values of 0.40–0.74 indicated fair to good reliability; and ICC values higher than 0.75 indicated excellent reliability [22]. For the comparison of ADC, slow component of diffusion (*D*), incoherent microcirculation (Dp), and *f* among the NP, PDACs, panNENs, and AIPs, data were analyzed by using the Kruskal–Wallis *H* test followed by a Steel–Dwass post hoc test. Receiver operating characteristic (ROC) analysis was then conducted to evaluate the diagnostic performance of IVIM-derived parameters. The areas under the ROC curve (AUC) were compared for significant differences between parameters, and the cut-off values with the largest Youden index, as well as sensitivity and specificity, were calculated. *p* values of < 0.05 were considered to indicate a significant difference. Statistical analysis was performed by using MedCalc (MedCalc Software, Mariakerke, Belgium).

Results

Patient characteristics

Patients with a cystic pancreatic lesion were excluded from this study ($n = 326$). Seventeen patients were additionally excluded owing to the lack of pathologic results ($n = 2$) and for the unsatisfactory quality of their imaging examination ($n = 15$). Finally, 57 patients (32 men, 25 women; mean age 62 years; range 40–79 years) with a pathology-proven solid pancreatic tumor or with AIP were enrolled in our study (34 PDACs, 18 panNENs, and 5 AIP); details are reported in Table 2. The diagnosis of pancreatic tumor was established in 25 cases after surgical resection and with 27 cases through fine-needle aspiration. The diagnosis of AIP was established by applying international consensus diagnostic criteria [21]; namely, in all cases AIP was diagnosed in the presence of (a) a long ($> 1/3$ length of the main pancreatic duct) stricture without marked upstream dilatation; (b) IgG4 $>$ 2x upper limit of normal value; and (c) rapid radiologically demonstrable resolution or marked improvement in manifestations.

The control group included 50 patients with normal pancreas (25 men, 25 women; mean age 56 years; range 28–76 years).

Table 2. Median size of pancreatic lesions and ROI areas

	Size (mm)	ROI area (mm^2)
NP ($n = 50$)	–	120 (50–410)
Pancreatic lesions ($n = 57$)	33.7 (12–141)	249 (26–1997)
PDAC ($n = 34$)	36.6 (14–66)	206 (90–1700)
panNEN ($n = 18$)	29.3 (12–141)	402 (26–1997)
AIP ($n = 5$)	34 (28–37)	95 (87.3–139)

Numbers in parentheses denote the range

Reliability of IVIM-derived parameters

Data are resumed in Table 3. The interobserver agreement of measurements for the pancreatic parenchyma was fair to good for ROI size and ADC (0.623 and 0.605, respectively) and excellent for IVIM-derived parameters. The interobserver agreement was excellent for pancreatic lesions. The overall interobserver agreement was excellent as well; the ICC values were 0.959 for ROI size, 0.860 for ADC maps, 0.937 for *D* maps, 0.968 for Dp maps, and 0.983 for *f* maps.

IVIM parameters

Median values of measured parameters for NP, PDACs, panNENs, and AIP are presented in Table 4; the results of the Steel–Dwass post hoc pairwise comparisons are

Table 3. Interobserver reliability of the measurements

Parameter	Normal pancreas	Pancreatic lesions	Overall
ROI size	0.623 (0.247–0.836)	0.988 (0.974–0.995)	0.959 (0.927–0.977)
ADC	0.605 (0.395–0.755)	0.941 (0.900–0.966)	0.860 (0.800–0.903)
D	0.755 (0.606–0.853)	0.962 (0.935–0.978)	0.937 (0.908–0.957)
Dp	0.943 (0.902–0.967)	0.963 (0.937–0.979)	0.968 (0.952–0.978)
f	0.933 (0.885–0.962)	0.989 (0.981–0.994)	0.983 (0.974–0.988)

Numbers in parentheses represent 95% confidence interval

Table 4. Median values of measured parameters for NP, PDAC, panNEN, and AIP

Parameter	NP (n = 50)	PDAC (n = 34)	panNEN (n = 18)	AIP (n = 5)	p value*
ADC[a]	1.37 (1.18–1.7)	1.41 (1.02–1.73)	1.28 (1.01–1.89)	1.24 (0.94–1.64)	0.109
D[a]	1.17 (0.9–1.47)	1.42 (0.87–1.97)	1.2 (0.54–1.56)	1.16 (0.84–1.76)	< 0.001
Dp[a]	29.99 (9.56–93.78)	10.23 (1.79–57.85)	28.9 (12.16–73.08)	10.62 (7.6–15.15)	< 0.001
f[b]	23.81 (14.16–34.35)	5.82 (2.12–18.84)	27.61 (3.22–80.83)	9.87 (4.18–11.60)	< 0.001

*According to the Kruskal–Wallis test for differences between NP, PDACs, panNENs, and AIP
[a]Data are expressed as the median value ($\times 10^{-3}$ mm^2/s), with ranges in parentheses
[b]Data are expressed as the median percentage, with ranges in parentheses

shown in Table 5. While ADC was not significantly different among NP and pancreatic lesions (p = 0.109), there were significant differences in D, Dp, and f among them (all $p < 0.001$; Fig. 1).

In particular, PDAC had significantly higher D and significantly lower Dp and f compared with NP (all $p < 0.001$; Figs. 1, 2) and with panNENs (p = 0.002, < 0.001, and < 0.001; Fig. 3). PDAC had also significantly lower f compared with AIP (p = 0.024).

Autoimmune pancreatitis had significantly lower Dp and f compared with NP (p = 0.003 and 0.024; Fig. 4) and panNENs (p = 0.029 and 0.023).

Diagnostic performance of IVIM-derived parameters

Table 6 summarizes the diagnostic performance of IVIM parameters in differentiating NP and pancreatic lesions.

Among IVIM-derived parameters, f had the highest AUC for differentiation of PDACs from NP, panNENs, and AIP (AUC = 0.989, 0.928, and 0.735, respectively). Despite this, there were no significant differences between Dp and f at pairwise comparison of ROC curves for differentiation between NP from PDACs and PDACs from panNENs (p = 0.23 and 0.74, respectively; Fig. 5).

Perfusion fraction had the highest AUC (1.000) for differentiation of AIP from NP; Dp showed the highest AUC for differentiation of panNENs from AIP (0.978). No significant differences were found at pairwise comparison of ROC curves between Dp and f for differentiation of AIP from NP and AIP from panNENs (p = 0.35 and 0.07, respectively; Fig. 5).

Discussion

Our study confirmed previous results regarding the usefulness of IVIM-DW imaging for the evaluation of solid pancreatic lesions. Perfusion-related IVIM-derived parameters allowed differentiation among NP and solid pancreatic lesions with high sensitivity and specificity. Perfusion fraction reached 100% sensitivity for differentiation of PDAC from NP and AIP from NP; specificity was higher than 80% for Dp and f in differentiating PDACs from panNENs and panNENs from AIP, as well as for f for differentiation of PDAC from AIP. Several previous studies reported that f, which represents the fractional volume of flowing water within a given image voxel [11], is the most significant IVIM-derived parameter for differentiation of solid pancreas lesions [13–17, 19, 20]. In our study, PDACs were characterized by significantly lower f compared with NP, panNENs, and AIP; moreover, f was significantly lower in AIP compared with NP and panNENs. In addition to the well-established role of f in lesion characterization, the results of our study suggest a role also for Dp, which expresses the collective motion of blood water molecules flowing within capillaries [11]. In our study, PDACs had significantly lower Dp compared with NP and panNENs, and AIP had significantly lower Dp compared with NP and panNENs. At pairwise comparison of ROC curves, there were no significant differences between Dp and f for differentiation between NP from PDACs, PDACs from panNENs, AIP from NP, and AIP from panNENs.

One of the most distinctive histologic features of panNENs is a very rich vascular network, compared with

Table 5. Results of the Steel–Dwass multiple comparison test

Parameter	NP vs. PDAC	NP vs. panNEN	NP vs. AIP	PDAC vs. panNEN	PDAC vs. AIP	panNEN vs. AIP
D	< 0.001	1	1	0.002	0.299	1
Dp	< 0.001	1	0.003	< 0.001	1	0.029
f	< 0.001	1	0.024	< 0.001	0.024	0.023

Data are *p* values

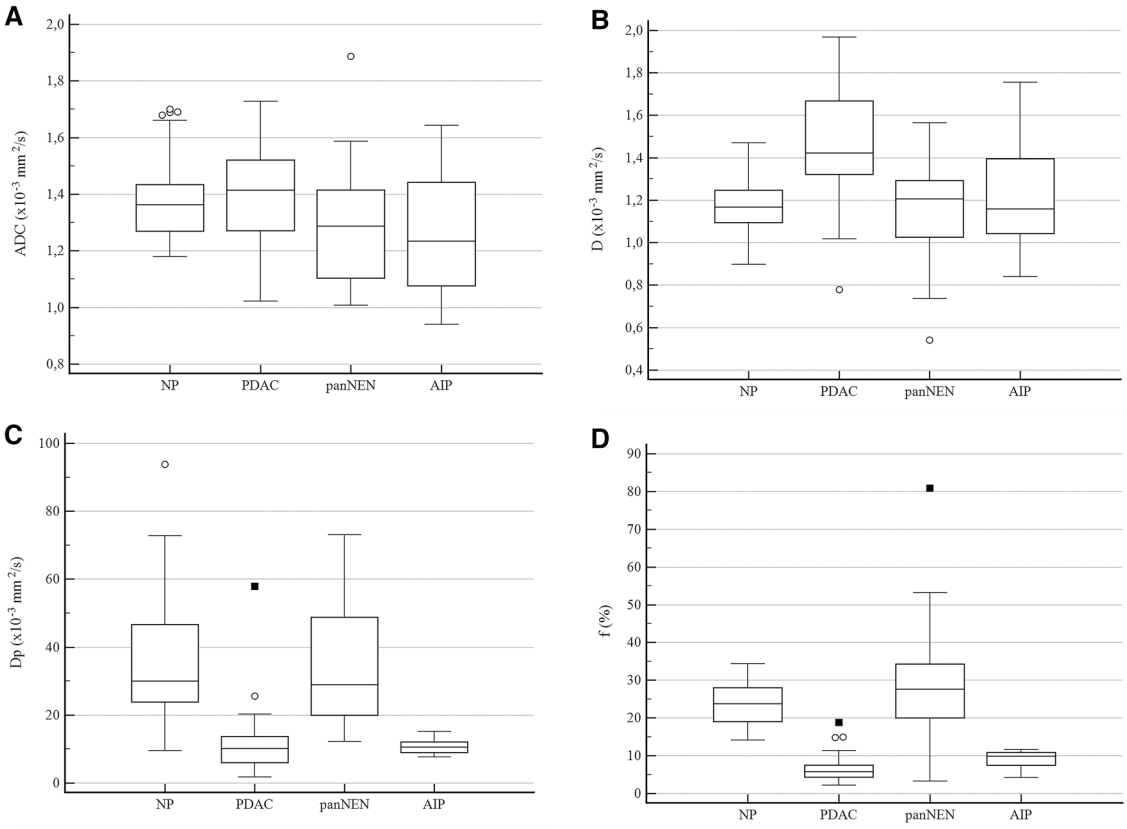

Fig. 1. **A–D** Boxplots of ADC (**A**), D (**B**), Dp (**C**), and f (**D**) for normal pancreas (NP), pancreatic ductal adenocarcinoma (PDAC), pancreatic neuroendocrine neoplasm (panNEN), and autoimmune pancreatitis (AIP).

very few vessels within abundant desmoplastic stroma found in PDACs. As happens with contrast enhancement, these differences in perfusion are the assumption for their differentiation using IVIM-DW imaging. Consistently, a previous study demonstrated a correlation between *f* and histologic microvessel density in PDAC and panNENs, indicating the dependency of *f* on the degree of tumor vascularity [16]. Pancreatic carcinomas and panNENs are usually easily differentiated at dynamic MR imaging, the former being markedly hypoenhancing compared with the latter. Yet, atypical presentations of panNENs are not uncommon on MR imaging [23, 24]: for instance, a previous study reported that up to 65% panNENs may lack a clear hyperenhancement on arterial phase images of dynamic MR [25], making their non-invasive differentiation from PDACs difficult. International consensus guidelines [26] suggest the measurement of chromogranin A and the use of 68 Ga PET/CT to support the radiological diagnosis of panNEN; moreover, core biopsy is mandatory for the classification of panNENs [26]. Although dynamic MR imaging still plays a major role in the characterization of focal pancreatic lesions, perfusion-related IVIM-derived parameters may represent an additional tool in non-invasive differentiation of solid pancreatic lesions showing an atypical imaging presentation.

Autoimmune pancreatitis is a benign disease of the pancreas, which usually presents with a diffuse enlargement of the gland [27, 28]. The diagnosis of AIP is assigned on the basis of international consensus diagnostic criteria previously proposed by Shimosegawa et al. [21], which include radiological, clinical, and biochemical data

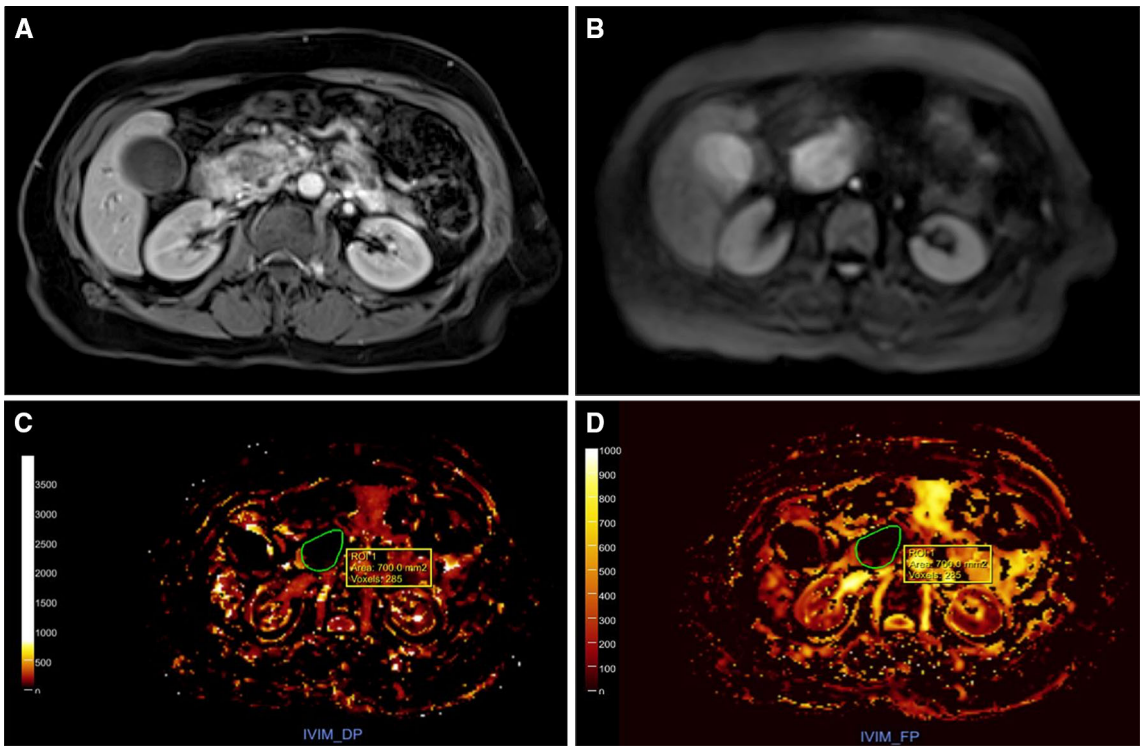

Fig. 2. **A**–**D** Findings in a 65-year-old female with PDAC. **A** Arterial phase axial T1-weighted VIBE image shows an ill-defined hypovascular lesion in the pancreas head. **B** On the axial diffusion-weighted image (**B** 800 mm/s^2), the mass shows high signal intensity. **C**–**D** On the Dp and f parametric maps, the mass (ROI) showed markedly reduced values.

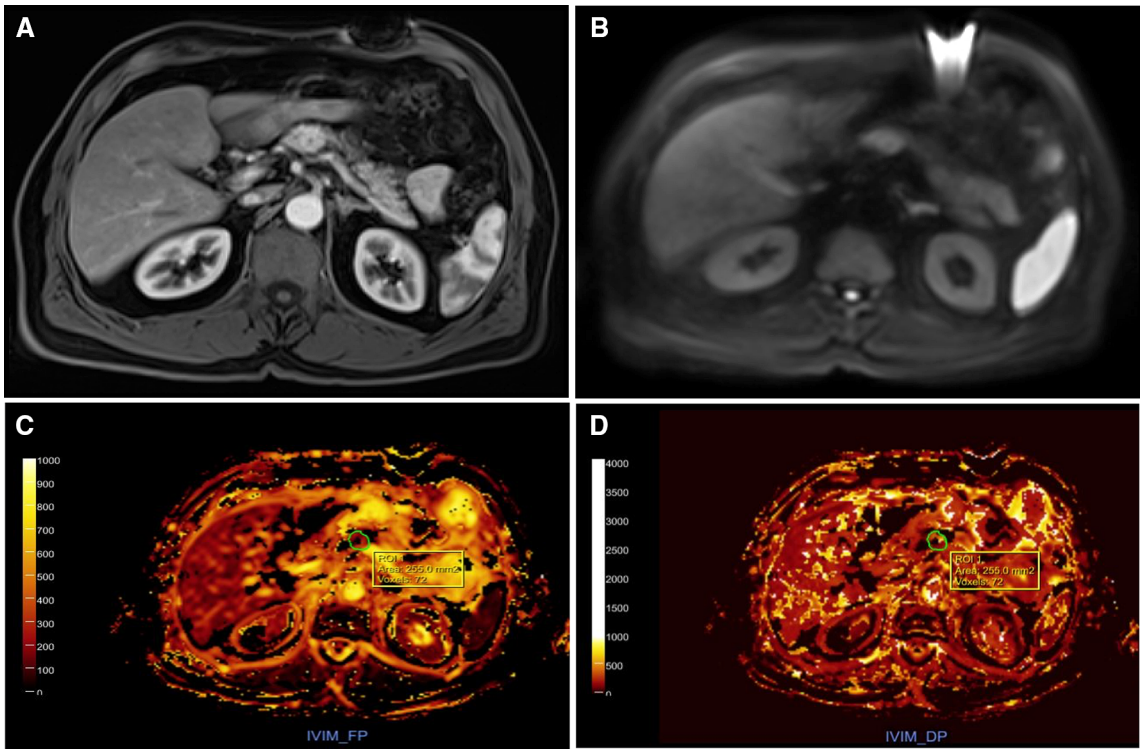

Fig. 3. **A**–**D** Findings in a 55-year-old male with panNEN. **A** Arterial phase axial T1-weighted VIBE image showing a well-defined hyperenhancing lesion in the pancreas body. **B** On the axial diffusion-weighted image (**B** 800 mm/s^2), the mass shows high signal intensity. **C**–**D** On the Dp and f parametric maps, the mass (ROI) showed increased values.

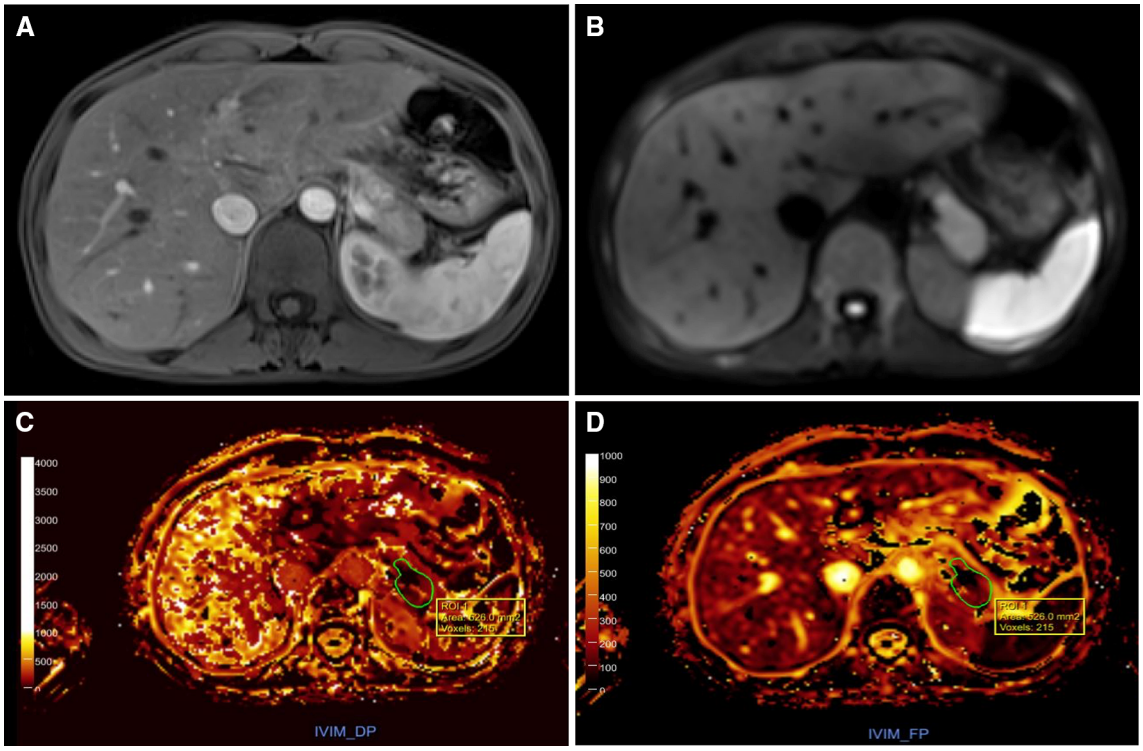

Fig. 4. **A–D** Findings in a 46-year-old female with AIP. **A** Arterial phase axial T1-weighted VIBE image showing a well-defined hypovascular lesion in the pancreatic tail. **B** On the axial diffusion-weighted image (**B** 800 mm/s^2), the mass shows high signal intensity. **C–D** On the Dp and f parametric maps, the mass (ROI) showed slightly reduced values.

Table 6. Results of ROC analysis

Comparison	AUC*	Cut off	Sensitivity (%)	Specificity (%)
NP vs. PDAC				
D	0.821 (0.722–0.896)	1.32	76.5	88
Dp	0.952 (0.883–0.987)	20.25	94.1	96
f	0.989 (0.937–1.000)	11.34	91.2	100
NP vs. AIP				
Dp	0.988 (0.913–1.000)	15.15	100	98
f	1.000 (0.935–1.000)	11.6	100	100
PDAC vs. panNEN				
D	0.789 (0.654–0.890)	1.29	77.8	76.5
Dp	0.905 (0.791–0.969)	17.93	83.3	88.2
f	0.928 (0.821–0.981)	9.31	94.4	85.3
PDAC vs. AIP				
f	0.735 (0.570–0.863)	8.37	80	82.3
panNEN vs. AIP				
Dp	0.978 (0.813–1.000)	15.15	100	88.9
f	0.911 (0.717–0.989)	11.6	100	83.3

*Numbers in parentheses represent 95% confidence intervals

(IgG4, IgG, and antinuclear antibody). In focal AIP there can be enough overlap in imaging features that differentiation from PDAC may be difficult, making necessary an extensive workup for pancreatic cancer including core biopsy and CA 19.9 dosage [21]. Albeit based on a small sample size, our results suggest that *f* may help in the non-invasive differentiation of AIP from PDAC, as this parameter may reflect the relatively well-preserved microvascularization in AIP as opposed to the very low microvascular density found within PDACs [16].

One issue that may limit the routine use of IVIM-DW imaging is the poor reliability of the measurements reported by several previous studies [29–31]. Differently from these studies, we reported a very high interobserver reliability for the measurements of IVIM-derived

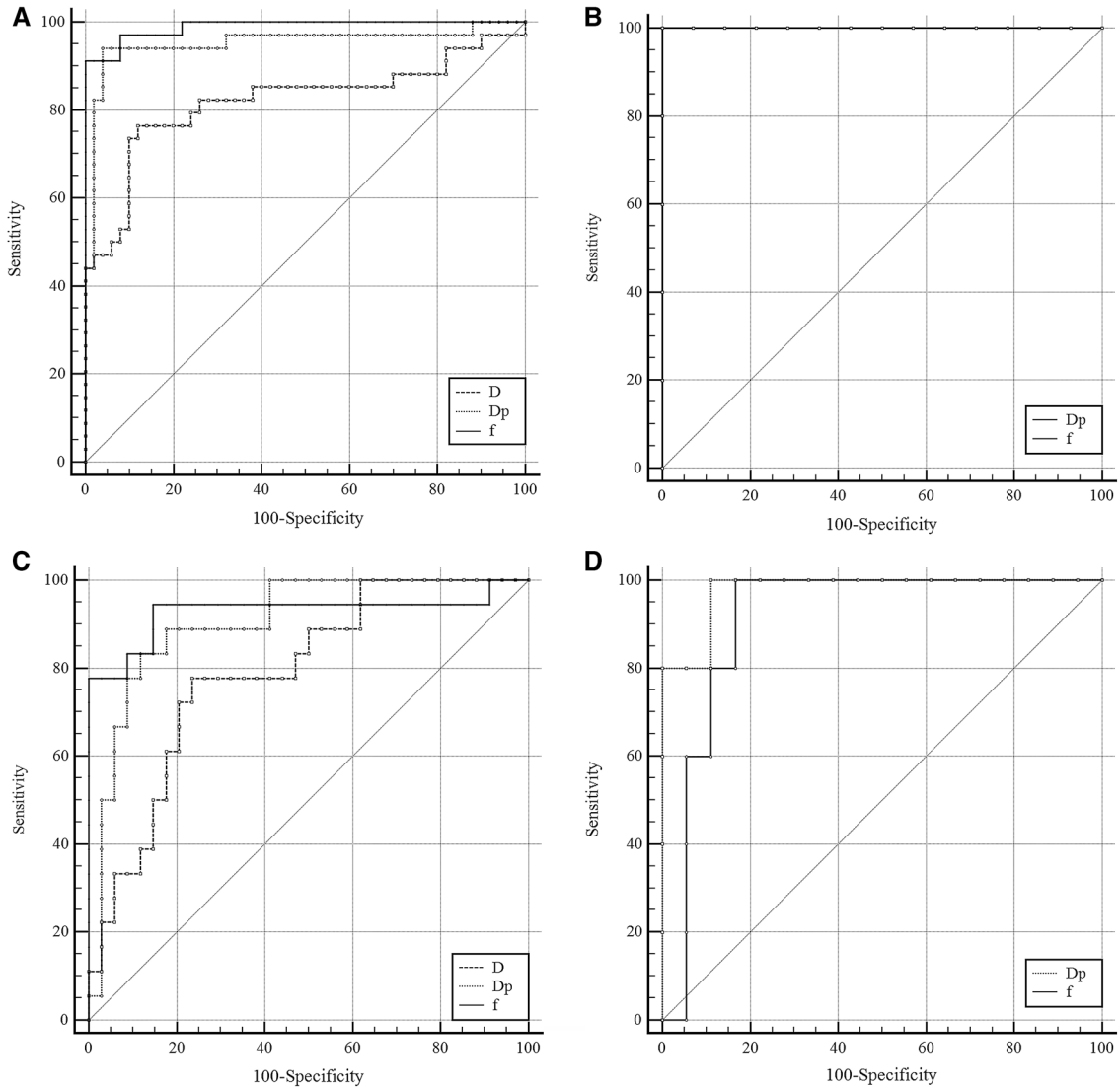

Fig. 5. **A–D** Comparison of ROC curves. **a** ROC curves of D, Dp, and f for differentiation of NP from PDAC. **B** ROC curves of Dp and f for differentiation of NP from AIP. **C** ROC curves of D, Dp, and f for differentiation of PDACS from panNENs. **D** ROC curves of Dp from f for differentiation of panNENs from AIP.

parameters, probably because this study was conducted in a high-volume center with high expertise in pancreatic imaging. Even if the interobserver reliability of the measurements reported by our study was lower for pancreatic parenchyma compared to pancreatic lesions, the overall reliability was excellent for all parameters, including Dp, which was found to have the lowest interobserver agreement among IVIM parameters in a study by Kim et al. [20].

The present study has several limitations: First, a very limited number of patients with focal AIP were included; therefore, our results in this subgroup of patients should be considered preliminary as determined using a small sample size. Second, because IVIM-DW images were acquired during free breathing, image misalignment due to organ motion may have influenced our results. However, as the pancreas is located in the retroperitoneum, the effect of respiratory motion may not be as relevant as in the other abdominal organs [1]. Furthermore, a previous study demonstrated a poorer reliability of breath-hold DW imaging in the measurement of ADC of PDACs compared to respiratory-triggered and free-breathing acquisitions [32].

In conclusion, our results suggest that IVIM-derived measurements, in particular Dp and *f*, are highly reproducible and are able to differentiate among NP and solid pancreatic lesions. Further studies are needed to better understand the real capability of IVIM-DW imaging in differentiating AIP from PDACs.

Compliance with ethical standards

Funding We state that this work has not received any funding.

Conflict of interest Riccardo De Robertis, Nicolò Cardobi, Silvia Ortolani, Paolo Tinazzi Martini, and Mirko D'Onofrio declare no economic relationships with any companies, whose products or services may be related to the subject matter of the article. Alto Stemmer is an employee of Siemens Healthcare GmbH. Robert Grimm is an employee of Siemens Healthcare GmbH, owns stocks of Siemens AG, and holds patents filed by Siemens.

References

1. Barral M, Taouli B, Guiu B, et al. (2015) Diffusion-weighted MR imaging of the pancreas: current status and recommendations. Radiology 274:45–63
2. Brenner R, Metens T, Bali M, Demetter P, Matos C (2012) Pancreatic neuroendocrine tumor: added value of fusion of T2-weighted imaging and high b-value diffusion-weighted imaging for tumor detection. Eur J Radiol 81:e746–e749
3. De Robertis R, Tinazzi Martini P, Demozzi E, et al. (2015) Diffusion-weighted imaging of pancreatic cancer. World J Radiol 7:319–328
4. De Robertis R, D'Onofrio M, Zamboni G, et al. (2016) Pancreatic neuroendocrine neoplasms: clinical value of diffusion-weighted imaging. Neuroendocrinology 103:758–770
5. Fukukura Y, Shindo T, Hakamada H, et al. (2016) Diffusion-weighted MR imaging of the pancreas: optimizing b-value for visualization of pancreatic adenocarcinoma. Eur Radiol 26:3419–3427
6. Yi WM, Chen ZE, Paul Nikolaidis MD, et al. (2011) Diffusion-weighted magnetic resonance imaging of pancreatic adenocarcinomas: association with histopathology and tumor grade. J Magn Reson Imaging 33:136–142
7. Lotfalizadeh E, Ronot M, Wagner M, et al. (2017) Prediction of pancreatic neuroendocrine tumour grade with MR imaging features: added value of diffusion-weighted imaging. Eur Radiol 27:1748–1759
8. De Robertis R, Cingarlini S, Tinazzi Martini P, et al. (2017) Pancreatic neuroendocrine neoplasms: magnetic resonance imaging features according to grade and stage. World J Gastroenterol 23:275–285
9. Kim M, Kang TW, Kim YK, et al. (2016) Pancreatic neuroendocrine tumour: correlation of apparent diffusion coefficient or WHO classification with recurrence-free survival. Eur J Radiol 85:680–687
10. Fattahi R, Balci NC, Perman WH, et al. (2010) Pancreatic diffusion-weighted imaging (DWI): comparison between mass-forming focal pancreatitis (FP), pancreatic cancer (PC), and normal pancreas. J Magn Reson Imaging 29:350–356
11. Le Bihan D, Breton E, Lallemand D, et al. (1988) Separation of diffusion and perfusion in intravoxel incoherent motion MR imaging. Radiology 168:497–505
12. Dixon WT (1988) Separation of diffusion and perfusion in intravoxel incoherent motion MR imaging: a modest proposal with tremendous potential. Radiology 168:566–567
13. Lemke A, Laun FB, Klauss M, et al. (2009) Differentiation of pancreas carcinoma from healthy pancreatic tissue using multiple b-values: comparison of apparent diffusion coefficient and intravoxel incoherent motion derived parameters. Invest Radiol 44:769–775
14. Klauss M, Lemke A, Grünberg K, et al. (2011) Intravoxel incoherent motion MRI for the differentiation between mass forming chronic pancreatitis and pancreatic carcinoma. Invest Radiol 46:57–63
15. Kang KM, Lee JM, Yoon JH, et al. (2014) Intravoxel incoherent motion diffusion-weighted MR imaging for characterization of focal pancreatic lesions. Radiology 270:444–453
16. Klau M, Mayer P, Bergmann F, et al. (2015) Correlation of histological vessel characteristics and diffusion-weighted imaging intravoxel incoherent motion-derived parameters in pancreatic ductal adenocarcinomas and pancreatic neuroendocrine tumors. Invest Radiol 50:792–797
17. Klauss M, Maier-Hein K, Tjaden C, et al. (2016) IVIM DW-MRI of autoimmune pancreatitis: therapy monitoring and differentiation from pancreatic cancer. Eur Radiol 26:2099–2106
18. Hecht EM, Liu MZ, Prince MR, et al. (2017) Can diffusion-weighted imaging serve as a biomarker of fibrosis in pancreatic adenocarcinoma? J Magn Reson Imaging 46:393–402
19. Ma C, Li Y, Wang L, et al. (2017) Intravoxel incoherent motion DWI of the pancreatic adenocarcinomas: monoexponential and biexponential apparent diffusion parameters and histopathological correlations. Cancer Imaging 17:12
20. Kim B, Lee SS, Sung YS, et al. (2017) Intravoxel incoherent motion diffusion-weighted imaging of the pancreas: characterization of benign and malignant pancreatic pathologies. J Magn Reson Imaging 45:260–269
21. Shimosegawa T, Chari ST, Frulloni L, et al. (2011) International consensus diagnostic criteria for autoimmune pancreatitis. Guidelines of the International Association of Pancreatology. Pancreas 40:352–358
22. Cicchetti DV (1994) Guidelines, criteria, and rules of thumb for evaluating normed and standardized assessment instruments in psychology. Psychol Assess 6:284–290
23. Corrias G, Monti S, Horvat N, et al. (2018) Imaging features of malignant abdominal neuroendocrine tumors with rare presentation. Clin Imaging 8:59–64
24. Lalwani N, Mannelli L, Ganeshan DM, et al. (2015) Uncommon pancreatic tumors and pseudotumors. Abdom Imaging 40:167–180
25. De Robertis R, Tinazzi Martini P, Cingarlini S, et al. (2014) Digital subtraction of magnetic resonance images improves detection and characterization of pancreatic neuroendocrine neoplasms. J Comput Assist Tomogr 41:614–618
26. Falconi M, Eriksson B, Kaltsas G, et al. (2016) ENETS consensus guidelines update for the management of patients with functional pancreatic neuroendocrine tumors and non-functional pancreatic neuroendocrine tumors. Neuroendocrinology 103:153–171
27. Hoshimoto S, Aiura K, Tanaka M, et al. (2016) Mass-forming type 1 autoimmune pancreatitis mimicking pancreatic cancer. J Dig Dis 17:202–209
28. Sugiyama Y, Fujinaga Y, Kadoya M, et al. (2012) Characteristic magnetic resonance features of focal autoimmune pancreatitis useful for differentiation from pancreatic cancer. Jpn J Radiol 30:296–309
29. Lee JH, Cheong H, Lee SS, et al. (2016) Perfusion assessment using intravoxel incoherent motion-based analysis of diffusion-weighted magnetic resonance imaging: validation through phantom experiments. Invest Radiol 51:520–528
30. Lee Y, Lee SS, Kim N, et al. (2015) Intravoxel incoherent motion diffusion-weighted MR imaging of the liver: effect of triggering methods on regional variability and measurement repeatability of quantitative parameters. Radiology 274:405–415
31. Andreou A, Koh DM, Collins DJ, et al. (2013) Measurement reproducibility of perfusion fraction and pseudodiffusion coefficient derived by intravoxel incoherent motion diffusion-weighted MR imaging in normal liver and metastases. Eur Radiol 23:428–434
32. Kartalis N, Loizou L, Edsborg N, Segersvard R, Albiin N (2012) Optimising diffusion-weighted MR imaging for demonstrating pancreatic cancer: a comparison of respiratory-triggered, free-breathing and breath-hold techniques. Eur Radiol 22:2186–2192